ORIGINAL ARTICLE

Characterization of organic anion transporting polypeptide 1b2 knockout rats generated by CRISPR/Cas9: a novel model for drug transport and hyperbilirubinemia disease

Xinrun Ma[†], Xuyang Shang[†], Xuan Qin,
Jian Lu, Mingyao Liu, Xin Wang[*]

Shanghai Key Laboratory of Regulatory Biology, Institute of Biomedical Sciences and School of Life Sciences, East China Normal University, Shanghai 200241, China

Abstract Organic anion transporting polypeptide 1B1 and 1B3 (OATP1B1/3) as important uptake transporters play a fundamental role in the transportation of exogenous drugs and endogenous substances into cells. Rat OATP1B2, encoded by the *Slco1b2* gene, is homologous to human OATP1B1/3. Although OATP1B1/3 is very important, few animal models can be used to study its properties. In this report, we successfully constructed the S*lco1b2* knockout (KO) rat model *via* using the CRISPR/Cas9 technology

Rat model

for the first time. The novel rat model showed the absence of OATP1B2 protein expression, with no off-target effects as well as compensatory regulation of other transporters. Further pharmacokinetic study of pitavastatin, a typical substrate of OATP1B2, confirmed the OATP1B2 function was absent. Since bilirubin and bile acids are the substrates of OATP1B2, the contents of total bilirubin, direct bilirubin, indirect bilirubin, and total bile acids in serum are significantly higher in *Slco1b2* KO rats than the data of wild-type rats. These results are consistent with the symptoms caused by the absence of OATP1B1/3 in Rotor syndrome. Therefore, this rat model is not only a powerful tool for the study of OATP1B2-mediated drug transportation, but also a good disease model to study hyperbilirubinemia-related diseases.

1. Introduction

Organic anion transporting polypeptides (OATPs), a family of 12 transmembrane domain glycoproteins, belong to the solute carrier (SLC) family, and transport important endogenous and exogenous substrates into cells[1]. The human OATP superfamily consists of 11 transporters subdivided into six families (OATP1−6), in which the OATP1B plays a crucial role[2]. The human OATP1B subfamily contains two members, OATP1B1 and OATP1B3, which are encoded by the *SLCO1B1* and *SLCO1B3* genes, respectively. The two proteins are not only mainly expressed in the sinusoidal membrane of the liver, but also are found in some tumor tissues[3−5]. The substrates of OATP1B1 and OATP1B3 cover a wide range, including endogenous substances such as bilirubin, bile acids and steroid hormones, as well as clinically used drugs like angiotensin II receptor blockers (sartans), hydroxymethylglutaryl (HMG)-CoA reductase inhibitors (statins), anticancer drugs (paclitaxel) and so on[6−8].

Since most drugs are metabolized by hepatocytes, the hepatic uptake rate mediated by OATP1B1/3 is a determinant of total clearance[9]. Inhibition of the activities of OATP1B1/3 can alter the systemic drug exposure and lead to serious adverse reactions[10]. Several clinical drug−drug interaction (DDI) cases of cyclosporine combined with statins were reported, as cyclosporine inhibited the activities of OATP1B1/3 and resulted in severe muscular toxicity of statins[11]. The U.S. Food and Drug Administration (FDA) guidelines for "in vitro metabolism- and transporter-mediated drug−drug interaction studies" also point out that DDI potentials mediated by OATP1B1 and OATP1B3 must be considered in the development of novel drugs[12]. On the other hand, the activities of OATP1B1 and OATP1B3 are closely related to human health. For example, the biotransformation of bilirubin, the substrate of OATP1B1/3, depends on the function of OATP1B1/3 *in vivo*[2]. If the function of two transporters is decreased or lost, the concentration of bilirubin in the blood will increase and lead to hyperbilirubinemia[13]. Rotor syndrome is an autosomal recessive inheritance of hyperbilirubinemia, caused an increase in conjugated bilirubin, which is due to the loss of activity of OATP1B1/3[14].

Human OATP1B1 and OATP1B3 also play significant roles in the progression of tumors like prostate cancer. One study showed that the uptake capacity of androgen in prostate cancer cells correlated with the activities of OATP1B1 and OATP1B3, and overexpressing OATP1B1 and OATP1B3 could increase cell viability[15]. In clinical surveillance, patients with the loss-of-function *SLCO1B3* 334GG/699AA haplotype showed longer median survival and improved 10-year survival rate[16]. At the same time, *SLCO1B3* may determine the progression time of the patients receiving androgen deprivation therapy for prostate cancer[17]. Therefore, OATP1B3 is a potential target for prostate cancer treatment, but there are no sufficient relevant studies at present. Thus, it is important to develop useful methods to study the functions of OATP1B1 and OATP1B3 in pathology and clinical medicine[18].

Knockout (KO) animal models lacking the key transporters are specific and fit for preclinical studies, especially pharmacological research[19]. OATP1B2 (also named SLCO1B2 or LST-1), encoded by the *Slco1b2* gene, has been identified in mice and rats, which is the closest ortholog of human OATP1B1 and OATP1B3[20]. The *Slco1b2* KO mouse model was generated in 2008 by homologous recombination[21,22]. In pharmacokinetic experiments, however, rats have many advantages that make them superior to mice, such as enough blood volume, strong tolerance and large sample size. In particular, rats are the preferred animal model to carry out hyperbilirubinemia research[23,24]. Therefore, we want to generate a *Slco1b2* KO rat model.

Clustered regularly interspaced short palindromic repeats (CRISPR)/CRISPR-associated protein-9 nuclease (Cas9) technology as the third generation of gene editing technology after zinc-finger nucleases (ZFN) and transcription activator-like effector nuclease (TALEN), presents distinct advantages in editing multiple genes simultaneously in the same cell[25]. Its core component is Cas9 protein, which combines mature CRISPR RNA (crRNA) to recognize and cleave exogenous nucleic acid molecules[26,27]. The cleavage of the target gene will cause double-strand breaks, and then initiate the repair method of non-homologous terminal conjugation, which will result in deletion, replacement or insertion mutations of cleavage sites, thus complete gene editing[28]. Currently, CRISPR/Cas9 system has been identified as one breakthrough technology in the biomedical research[29].

In this study, we knocked out the *Slco1b2* gene in rats by using the CRISPR/Cas9 system, and successfully obtained the *Slco1b2* KO rat model. This model can be applied to pharmacokinetics studies. At the same time, the model can be used as a disease model of hyperbilirubinemia−Rotor syndrome.

2.   Materials and methods

2.1.   Animals

Male and female Sprague—Dawley (SD) rats were purchased from National Rodent Laboratory Animal Resources (Shanghai, China). Animals were fed in a barrier free of specific pathogens and allowed to eat and drink freely. The barrier was a temperature and humidity controlled environment with 12-h light/dark cycles. All the animal experiment protocols in this study were approved by the Ethics Committee on Animal Experimentation of East China Normal University (Shanghai, China).

2.2.   Chemicals and reagents

The oligos (60 bp, containing *Slco1b2* knock out target-site) and all primers for PCR/Q-PCR were synthesized by Biosune Biotechnology Co., Ltd. (Shanghai, China). KOD-plus-Neo polymerase was purchased from Toyobo (Osaka, Japan). SYBR Premix Ex Taq and Prime Script RT Reagent Kit were bought from Takara (Dalian, China). T7 endonuclease I (T7E I) was purchased from New England Biolabs (Ipswich, MA, USA). Phenol:chloroform:isoamyl alcohol (25:24:1, *v/v/v*) was purchased from Amresco (Cleveland, OH, USA). Bicinchoninic acid kit was purchased from Thermo Scientific (Waltham, MA, USA). The agarose gel recovery kit was bought from Generay Biotech Co., Ltd. (Shanghai, China). A primary antibody for OATP1B2 was purchased from Santa Cruz Biotechnology (Santa Cruz, CA, USA), and glyceraldehyde 3-phosphate dehydrogenase (GAPDH) was purchased from Abcam (Cambridge, UK). The fluorescence-conjugated secondary antibody to rabbit IgG and mouse IgG were bought from Cell Signaling Technology (Boston, MA, USA). Pitavastatin was obtained from MedChemExpress (Monmouth Junction, NJ, USA).

2.3.   Target-site selection

The *Slco1b2* gene sequence of *Rattus norvegicus* (Norway rat) was obtained from NCBI (https://www.ncbi.nlm.nih.gov/pmc/), and exon regions were sequentially labeled (from 1st to 15th). In order to completely knock out the target gene, the selected target is at the first exon of the rat *Slco1b2* gene. The first exon sequence was input into the online website (https://benchling.com/) to obtain an 18 bp target sequence followed by a protospacer adjacent motif (PAM) site (5′-NGG-3′) in the 3′ end. The target sequence is 5′-GCAAACAAGGTTCTGCGA-3′. PAM site is TGG.

2.4.   In vitro single guide RNA (sgRNA) template synthesis and transcription

The 60 bp oligo fragment containing the T7 promoter and 18 bp target sequence (5′-GATCACTAATACGACTCACTATAGGGCA AACAAGGTTCTGCGAGTTTTAGAGCTAGAAAT-3′) was synthesized by Biosune Biotechnology Co., Ltd. (Shanghai, China). Using this product, the sgRNA double-stranded template was synthesized by overlapping PCR using KOD-plus-neo polymerase, and then transcribed by the T7 transcription kit. The sgRNA of *Slco1b2* gene was extracted and purified by phenol/chloroform method, and then stored in −80 °C refrigerator for later experimentation.

2.5.   Embryo microinjection

First, healthy adult male rats (over 8 weeks old) were sterilized and caged with healthy adult female rats (over 8 weeks old). The female rats with vaginal suppositories were used as pseudo-pregnant rats for subsequent experiments. Then, the normal adult female rats were injected with pregnant mare serum gonadotropin (PMSG) and human chorionic gonadotropin (HCG) for super-ovulation and then mated and conceived. Female rats that had been mated successfully were sacrificed, and the embryos were taken out and cultured in culture medium for 2 h in a 37 °C, 5% CO_2 incubator. Finally, the sgRNA template (25 ng/μL) and Cas9 mRNA (50 ng/μL) were co-injected into the cytoplasm of the embryos by microinjection technique. The concentration ratio of sgRNA to Cas9 mRNA was 1:2. After several hours of culture, the surviving embryos were transplanted into the fallopian tube of the pseudo-pregnant rats. The pseudo-pregnant rats were returned to the cage for normal feeding.

2.6.   Genotype identification

2.6.1.   Genotype identification of F0 offspring rats
The newborn rats were cut the toes and randomly numbered when they grew to a week or so. The genomic DNA was extracted by phenol/chloroform method, and specifically amplified 600 bp sequences flanking the target site by the primers of *Slco1b2* (Table 1) with Easy-Taq DNA polymerase. Gradient annealing of 10 μL PCR product was carried out under the condition that 95 °C was maintained for 5 min, and each cycle decreased by 1 °C for 60 cycles, each cycle lasted for 30 s. The annealed products were digested in 37 °C incubator for 30 min using 0.1 μL T7 endonuclease I (T7E I). T7E I could recognize and cleave the mismatched bases with insertion or deletion mutations, and then multiple bands can be seen when electrophoresed on a 1.5% agarose gel. The positive PCR products (showed multiple bands) were recovered and purified by the agarose gel recovery kit and ligated into pMD18-T vector according to the TA cloning kit, and then the clones were sequenced to determine the accurate gene editing results. Although the clones tested can only reflect part of the genetic editing in the rat genome, we mainly use them as a reference to select the rats needed for subsequent experiments. The mutation is available only if there were insertion or deletion of non-three-integer multiple bases occurred on the exon. In addition, in order to simplify future sequence analysis, gene editing with replacement mutations or confusion of sequencing maps was discarded.

2.6.2.   Genotype identification of F1 and F2 offspring rats
The F0 offspring, carrying the available mutations, were caged with wild type (WT) rats and the progeny obtained were F1 generation. The genomic DNA of F1 rats was sequenced and analyzed. The healthy adult F1 male and female rats with the same mutation were selected for mating and breeding to obtain F2 generation. The genomic DNA of F2 rats were performed by PCR amplified sequences flanking the target site, and data was analyzed by DNAman (Lynnon Biosoft, San Ramon, CA, USA).

2.7.   Off-target site detection

The *Slco1b2* gene target sequence was input into the online target prediction website (https://benchling.com/) to obtain potential off-target sites. Three sites (Table 2), with a relative high probability of off-target (score>2.0) were selected, and 300 bp sequences of

Table 1 Primers accurate information for target and off-target sites.

Primer name	Primer sequence (5′—3′)	Product length (bp)	Temperature (°C)
Slco1b2-genotyping-S	CAGGGTAGACGACCATT	631	56
Slco1b2-genotyping-A	CTTTCTGCCAGGTGTTTT		
Slco1b2-off 1-S	TTGACCATCACAACGGAATC	475	60
Slco1b2-off 1-A	CTGGGTGAATGAACTACTTGC		
Slco1b2-off 2-S	TGTGGGGCCAGAGGACAG	445	62
Slco1b2-off 2-A	AGTTGGATGAAGATGAGGACTG		
Slco1b2-off 3-S	GGGGAACCAAGATGTGAA	410	60
Slco1b2-off 3-A	GAGCAAATAAGAAAGTCAGGAA		

upstream and downstream potential sites were found in NCBI (https://www.ncbi.nlm.nih.gov/pmc/), respectively. Based on the above sequences, primers (Table 1) for PCR were designed using Primer Premier. Three genome of KO rats were randomly selected to amplify the potential off-target sites using the primers in Table 1 and Easy-Taq DNA polymerase. The products were digested with T7E I and then performed by agarose gel electrophoresis (As described in Section *2.6.1*). If there is off-target effect, two bands appear after electrophoresis.

2.8. Detection of protein OATP1B2 expression

Since OATP1B2 is almost specifically expressed in the liver except in some tumor tissues, the expression of OATP1B2 in the livers of WT and KO rats was detected by Western blot and immunohistochemistry, respectively. Rats (8 weeks old) were killed by CO_2 asphyxiation and the livers were carefully separated and frozen in -80 °C for further processing.

2.8.1. Western blot analysis
Every unit of liver (0.1 g) was added with 400 μL lysate, containing RIPA, protease inhibitor, phosphatase inhibitor and phenylmethanesulfonyl fluoride. The sample was homogenized by Automatic Sample Rapid Grinding Instrument (JXFSTPRP-24, shanghai, China) and pyrolyzed at 4 °C for 2 h to extract total protein. Protein concentration was detected by using the Bicinchoninic acid Kit. Sodium dodecyl sulfate polyacrylamide gel electrophoresis (SDS-PAGE) was performed with 60 μg protein sample per well, and then the protein was transferred to a nitrocellulose (NC) membrane and blocked with 5% skim milk powder in Tris-buffered saline Tween 20 (TBST) buffer for 1 h. After incubation of primary antibody, mouse anti-OATP1B2 (sc-376904, diluted 1:200) and rabbit anti-GAPDH (AB181602, diluted 1:10,000) at 4 °C overnight, the anti-mouse/rabbit secondary antibody (diluted 1:10,000) were incubated for 1 h in the dark, and the blots were scanned by Odyssey imager system (LI−COR, Lincoln, NE, USA). The GAPDH was used as a loading control.

2.8.2. Immunohistochemical analysis
The liver tissue was carefully cut into pieces (1 cm × 1 cm × 0.5 cm), soaked in 4% paraformaldehyde, and completed the preparation according to the standard paraffin section immunohistochemical process. The primary antibody, mouse anti-OATP1B2 (sc-376904, diluted 1:100) was incubated at 4 °C overnight, and the secondary antibody used horseradish peroxidase (HRP)-labeled goat anti-mouse IgG (GB23301, diluted 1:200) was incubated at room temperature for 50 min. Color was developed using the immunohistochemistry kit 3,3-diaminobenzidine (DAB) chromogenic reagent, and the nucleus was counterstained with hematoxylin.

2.9. Detection of physiological condition

In order to detect whether the physiological condition changed in the *Slco1b2* KO rat, blood samples from WT and KO female and male rats (4-week-old and 8-week-old) were taken by the tail vein, and the serum physiological indexes were detected by ADICON Clinical Laboratories (Shanghai, China). Liver function indicators include total protein (TP), albumin (ALB), globulin (GLB), albumin/globulin ratio (A/G), total bilirubin (TBL), direct bilirubin (DBL), Indirect bilirubin (IBIL), aspartate aminotransferase (AST), alanine aminotransferase (ALT), aspartate aminotransferase/alanine aminotransferase (AST/ALT), alkaline phosphatase(ALP), γ-glutamyltranspeptidase (R-GT) and total bile acid (TBA). Renal function indicators include blood urea nitrogen (BUN), creatinine (CR), uric acid (UA). Blood lipid indexes include triglyceride (TG), total cholesterol (T-CH), high density lipoprotein cholesterol (HDL-C) and low density lipoprotein cholesterol (LDL-C). Glucose (GLU), a commonly used indicator of physiological status, was also detected. In addition, Haemotoxylin and Eosin (HE) staining according to standard procedures was used to detect whether the liver was abnormal.

2.10. Detection of compensatory effects

Total RNA in the livers of WT and KO rats were extracted using the Trizol method according to the instructions. After measuring

Table 2 Details for potential off-target sites examined.

Match name	Location	Spacer + PAM	Off-target score
Slco1b2-sgRNA	Chr4-175819244	GCAAACAAGGTTCTGCGATGG	100.00
Slco1b2-off-1	Chr1-13544758	GCAAACAAGGTTCTGCGGTAG	19.60
Slco1b2-off-2	Chr14-3156777	GCAAACAGAGTTCTGCGAAGG	3.19
Slco1b2-off-3	Chr7-114058847	GGAGACAGGGTTCTGCGAGGG	2.67

Chr, chromosome.

the concentration with nano-drop 2000 spectrophotometer (Thermo Fisher Scientific, Waltham, MA, USA), the RNA (total 2000 ng) was quantitatively reverse transcribed into cDNA using the Takara RT kit (RR036A). The primary efflux and absorption transporters were detected by real-time quantitative PCR was performed using Quant Studio 3 Real-Time PCR System (Thermo Fisher Scientific). The efflux transporters included *Abcc1*, *Abcc2*, *Abcc3*, *Abcb1a*, *Abcb1b*, *Abcg2*, *Abcg5*, *Abcg8*, and *Abcb11*, while the absorbing transporters included *Slco1b2*, *Slco1a1*, *Slco2a1*, *Slco1a2*, *Slco2b1*, *Slc22a1*, *Slc22a3*, *Slc22a7*, *Slc22a8*, and *Slc10a1*. Primers information is listed in the Supporting Information Table S1. The *β*-actin was set as the internal reference.

2.11. Pitavastatin pharmacokinetic studies in WT and KO rats

In order to determine whether the protein OATP1B2 lost its function in KO rats, pitavastatin, recommended by FDA, was used as the substrate of OATP1B2 to detect whether the pharmacokinetic behavior changed in 8-week-old KO male rats. Pitavastatin powder was dissolved with 5% dimethyl sulfoxide (DMSO) and 95% methylcellulose (MC) as solvents. The dosage was 5 mg/kg and the volume was 4 mL/kg, and the final concentration of pitavastatin was 1.25 mg/mL. The dosage was obtained according to the clinical dosage and the predicted experimental results[30]. After fasting for 12 h, pitavastatin was given to rats intragastrically. Blood samples were collected through tail vein at 0.17, 0.5, 1.0, 1.5, 2.0, 3.0, 4.0, 6.0, 8.0, 12.0, and 24.0 h after administration. Samples were centrifuged at $8000 \times g$ for 10 min, and the plasma was collected and stored at -20 °C for subsequent experiments.

2.12. Quantification of pitavastatin in plasma samples by LC−MS/MS

Before quantification, the plasma samples were thawed at room temperature and treated with liquid−liquid extraction. One hundred microliter of each plasma sample was added with 10 μL methanol, 10 μL of internal standard solution (IS, 100 ng/mL mebendazole in acetonitrile) and 800 μL of ethyl acetate. The mixture was mixed thoroughly and centrifuged at $14,000 \times g$ for 10 min. An aliquot of 600 μL upper organic layer was transferred to a new 1.5 mL tube afterwards, and dried with a gentle flow of hot nitrogen. The residue was then reconstituted with 100 μL methanol/water (1:1, *v/v*) and centrifuged at $14,000 \times g$ for 10 min. Finally 80 μL of supernatant was used for LC−MS/MS analysis.

The LC−MS/MS system consisted of an Agilent 1290 HPLC and a 6460 triple quadrupole mass spectrometer coupled with an Agilent Jet Stream ESI ion source (Agilent Technologies, Santa Clara, CA, USA). Chromatography separation was performed on a Zorbax Eclipse Plus C18 column (50 mm × 2.1 mm, 1.8 μm, Agilent Technologies), using a mobile phase system of water (A) and methanol (B) both containing 0.1% formic acid (*v/v*). The flow rate was 0.2 mL/min and the injection volume was 2 μL. The gradient elution program was used as follows: 0−0.5 min, 45% B; 0.5−3 min, 45%−95% B; 3−3.5 min, 95% B; 3.5−3.7 min, 95%−45% B; 3.7−5.5 min, 45% B. Pitavastatin and IS were both monitored in positive ESI mode, with the ion transition of 422.1 → 22.1I and 296.1 → 264.1, respectively.

2.13. Statistical data analysis

All data were presented as mean ± SD. All the graphs were plotted by GraphPad Prism 6.0 (GraphPad Software Inc., San Diego, CA, USA). Statistical analysis between different groups was performed using the two-tailed *t*-test. The difference was considered to be statistically significant if $P < 0.05$. The pharmacokinetic parameters of pitavastatin were calculated by Win-Nonlin software version 5.2.1 (Pharsight Corporation, Mountain View, CA, USA) based on the non-compartmental model.

3. Results

3.1. Gene analysis of Slco1b2 KO rats

In the genetic identification of F0 generation rats, the T7E I assay and sequence analysis were used. As shown in Fig. 1A, in the absence of T7E I (T7E I⁻) cleavage, the bands of 13# and 31# rats were significantly lower than the WT, and 2#, 18#, 29#, and 36# showed obvious two bands, indicating that there may be a deletion of longer fragments. After sequencing analysis, it was confirmed that more than 100 bp base deletion occurred in the above rat genome. However, because of the occurrence of non-effective editing in 18# and 31#, and a replacement mutation occurred in 2#, 13#, 29#, and 36#, the above rats were abandoned. Sequence analysis of other genomes (3#, 5#, 7#, and etc.) revealed that 10#, 14#, 15#, 20#, 21#, 22#, and 30# contained effective editing. But in order to simplify the future workload, we randomly selected 10#, 15#, and 21#F0 rats for subsequent experiments. Part of the sequencing results are shown in the Supporting Information Table S2.

The genomic DNA of F1 rats was sequenced and analyzed. The healthy adult F1 male and female rats with the same mutation were selected for mating and breeding to obtain F2 generation. The possible genotypes of the F2 generation are WT rats, homozygous KO rats, and heterozygous (HZ) rats. After specific amplification of the F2 generation rat genomic DNA, sequencing analysis was performed. As shown in Fig. 1B, individuals with a homozygous deletion of 11 bp were obtained.

3.2. Off-target analysis

Since CRISPR/Cas9 system allows one to three base mismatches when sgRNA paired with target, it may lead to the combination of sgRNA and non-target sequence, resulting in off-target effect. Therefore, it is necessary to detect the off target in gene-editing rats. As shown in Fig. 2, all the bands were single, bright and uniform in size, indicating that the *Slco1b2* KO rats did not have off-target effects at the detected off-target sites.

3.3. Expression of OATP1B2 in WT and KO rats liver

The expression of OATP1B2 in the liver of WT and KO rats was checked by Western blot and immunohistochemistry, respectively. As shown in Fig. 3A, the OATP1B2 protein was completely absent in the liver of KO rats. In Fig. 3B, in WT rats, OATP1B2 was highly expressed on the sinusoidal membrane of the liver (shown in brown), while there was almost no positive result in the liver of KO rats. These results confirmed that OATP1B2 protein was absent completely in KO rats, suggesting that the KO model was successfully constructed.

3.4. Detection of physiological conditions of WT and KO rats

Since some important endogenous substances, such as bilirubin and bile acids, are substrates of OATP1B2, it is necessary to detect
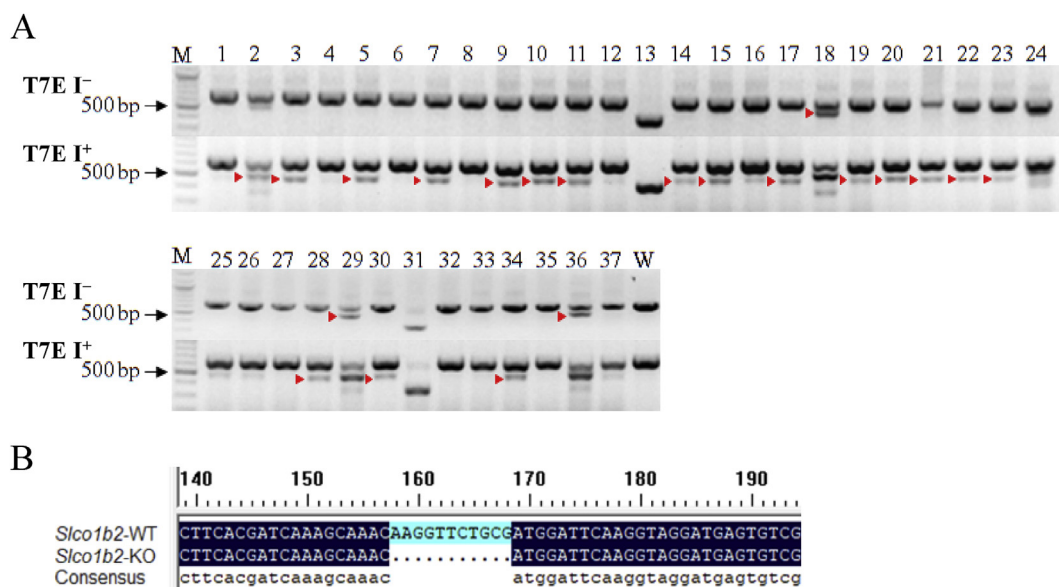
Figure 1 Genotype identification of offspring. (A) The mutations in F0 generation were detected by T7E I digestion using PCR products amplified from F0 rat tail genomic DNA by Primer. T7E I⁻, before T7E I digestion. T7E I⁺, after T7E I digestion. "▶", mutation band. WT, wild type as negative control. M, DNA molecular weight marker. (B) Gene sequence near the target in WT and *Slco1b2* KO rats. "…", missing sequence.

whether the physiological indexes of *Slco1b2* KO rats change and whether the rats grow and breed normally. We detected the physiological conditions of WT and KO rats by serum analysis and HE staining.

In addition, the *Slco1b2* KO rats may be used as a disease model of Rotor syndrome, and the main disease characteristics are the increase of DBL and TBL in adolescents. Therefore, we randomly selected WT and KO rats (4-week-old and 8-week-old) to perform serum tests of liver function. As shown in Fig. 4, the TBL, DBL and IBIL increased significantly in male KO rats at both 4 (Fig. 4A) and 8 (Fig. 4B) weeks old compared with WT rats. Among them, the 4-week-old rats increased 2.46-, 4.55-, and 1.63-fold, respectively. And the 8-week-old rats increased 2.18-, 5.26-, and 1.62-fold, respectively. These results indicate that *Slco1b2* KO rats can mimic Rotor syndrome with a phenotype similar to humans. In particular, the TBA increased significantly by 3.93- and 7.98-fold in 4- and 8-week old KO rats, respectively. Moreover, ALB in 4-week-old and AST in 8-week-old KO rats were showing statistically significant differences. However, these parameters are still within the normal range of the rat, and there is no clinical significance. Except for the above indexes, there was no significant difference in other liver function indexes between KO and WT rats. At the same time, as shown in Fig. 5A, there was no significant difference in renal function indications, blood lipid indications and glucose between KO and WT rats. Furthermore, we also tested female rats and the results were consistent with those of male rats (data not shown).

HE staining was performed on the liver of 4-week-old and 8-week-old KO and WT rats to observe the morphology of hepatocytes. There was no significant difference in liver morphology between WT and KO rats at 4 weeks old (Supporting Information Fig. S1). However, in the slices of liver tissues of 8-week-old WT rats (Fig. 5B), the central lobular area showed a radial arrangement of hepatic cords from the central vein outward, with normal cell morphology, uniform cytoplasm and orderly arrangement. In contrast, the structure of hepatocyte cord in the 8-week-old KO rat

was blurred and disordered, and the hepatic sinusoids were enlarged, suggesting slight damage to the liver, which may be related to the long-term high content of bilirubin and bile acid.

3.5. Compensatory expression of major transporters in WT and KO rats

In order to detect the compensatory expression of other major transporters in rats after *Slco1b2* gene knockout, we detected the mRNA levels of major uptake and efflux transporters by real-time quantitative PCR. The data showed, except for the target gene *Slco1b2*, there was no significant difference in mRNA levels of other transporters (Supporting Information Fig. S2). Therefore, the transporters detected did not compensate at the transcriptional level in KO rats.
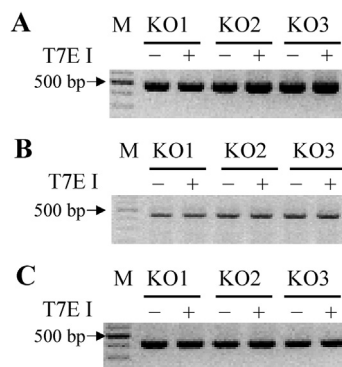

Figure 2 Off-target analysis in *Slco1b2* KO rats. Three off target sites for *Slco1b2* sgRNA were selected for T7E I enzyme cleavage. (A) *Slco1b2*-off target-1, (B) *Slco1b2*-off target-2, (C) *Slco1b2*-off target-3 analysis of KO rats ($n = 3$). T7E I⁻, before T7E I digestion; T7E I⁺, after T7E I digestion. M, DNA molecular weight marker.
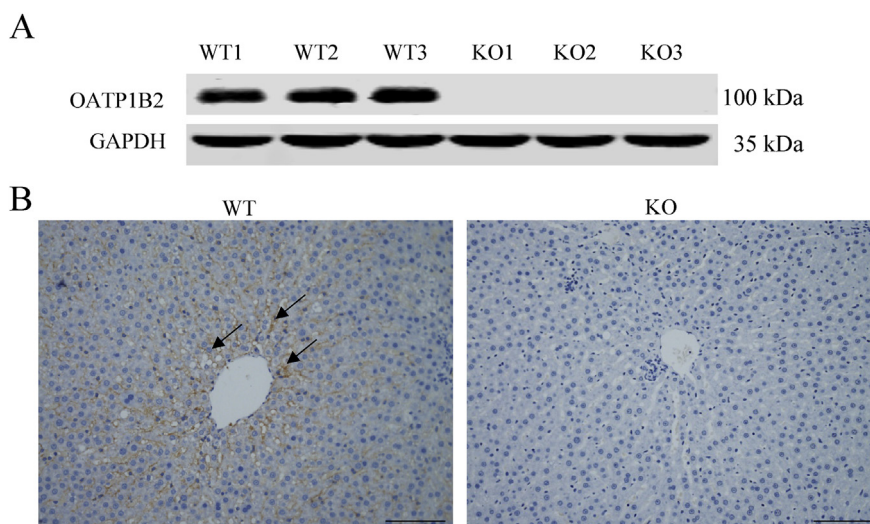
A

B

Figure 3   Analysis of OATP1B2 protein expression in WT and KO rats. (A) Western blot analysis of OATP1B2 protein expression level in the livers of WT and KO rats ($n = 3$). The molecular weight of OATP1B2 is about 100 kDa. The molecular weight of GAPDH (the internal reference) is about 35 kDa. (B) Immunohistochemistry analysis of OATP1B2 protein expression in the livers of WT and KO rats. Positive results are shown in brown (↑). Scale bars, 200 μm in length.

3.6.   Pharmacokinetics of pitavastatin in WT and KO rats

To further detect whether the function of OATP1B2 in KO rats is affected, we used pitavastatin, a specific OATP1B2 substrate recommended by FDA, to conduct pharmacokinetic experiments in WT and KO rats by oral administration (Fig. 6). The dose of pitavastatin (5 mg/kg) is based on clinical doses and preliminary experiments. Compared with WT rats, the area under the time−plasma concentration curve (AUC), both $AUC_{0-24\ h}$ and AUC_{0-inf} of KO rats were significantly increased by 68.8%, while the apparent volume of distribution/bioavailability (V_d/F) and clearance/bioavailability (CL/F) were significantly decreased by 39.8% and 38.5%, respectively (Table 3). Although peak time (T_{max}), peak concentration (C_{max}) and mean residence time (MRT) had no significant differences, they all had trends of increase. The results showed that the pharmacokinetic behavior of pitavastatin in KO rats was changed, especially a significant increase of *in vivo* exposure. Therefore, the function of OATP1B2 was absent in KO rats.

4.   Discussion

In recent years, the studies on OATP1B1 and OATP1B3 have become more and more popular because of their transport function of important endogenous and exogenous substances[11]. The past research mainly focused on transporter-involved drug safety evaluation, drug resistance and disease progression[9,31,32]. The *in vitro* and *in vivo* models for studying the role of OATP1B in drug research are limited with many drawbacks. *In vitro* cell models mainly include primary cells and transfected cells. However, cell culture conditions are strict and lack regulatory pathways, which do not reflect the real situation of complex living organisms[33,34]. *In vivo* models include organ perfusion model, inhibitor inhibiting transporter activity and gene knockout model. However, both the organ perfusion model and the use of inhibitors have the disadvantages of low specificity of inhibitors and high cost[35].

Gene knockout models have attracted more and more attention in recent years because they can better reflect the function of transporters under physiological conditions. In 2008, *Oatp1b2*-null mice were engineered by homologous recombination and their phenotype was characterized[21,22]. However, due to technical limitation such as the difficulty in obtaining and culturing rat embryonic stem cells, there has been no rat model with *Slco1b2* gene knockout to date. Compared with mice, rats have many advantages in pharmacokinetic and toxicological studies, such as large size and easy to handling, adequate blood volume and strong tolerance. In particular, the rat model can more accurately and comprehensively reflect the absorption, distribution, metabolism and excretion of drugs or compounds *in vivo*[36−38]. In addition, current research on hyperbilirubinemia has found that the rats are the preferred animal model[23,24]. Therefore, *Slco1b2* knockout rats can be used as the disease model of Rotor syndrome. The early gene knockout technology based on the principle of homologous recombination is very difficult to generate rat models because of the low efficiency and long experimental period. However, the emergence of CRISPR/Cas9 technology has brought light to the gene editing of rats[25]. CRISPR/Cas9 system is a new generation of gene editing technology. Compared with the traditional homologous recombination method, CRISPR/Cas9 has many advantages, such as easy operation, short cycle, low cost, high success rate and no species limitation[39]. Therefore, this study selected CRISPR/Cas9 technology to successfully generate the *Slco1b2* KO rat model for the first time.

Compared with WT rats, there was no expression of OATP1B2 protein in the liver of KO rats by the Western blot and immunohistochemistry analysis (Fig. 3). We also detected the mRNA expression of other transporters to determine whether there were compensatory effects by using the screening method of Q-PCR. The results showed that the transporters detected did not compensate at the transcriptional level in KO rats. Furthermore, we used the OATP1B2 substrate pitavastatin to verify the change of OATP1B2 function *in vivo*. The suspension of pitavastatin in CMC-Na was used in the pharmacokinetic study *via* the oral administration, which might be the cause for large deviation in
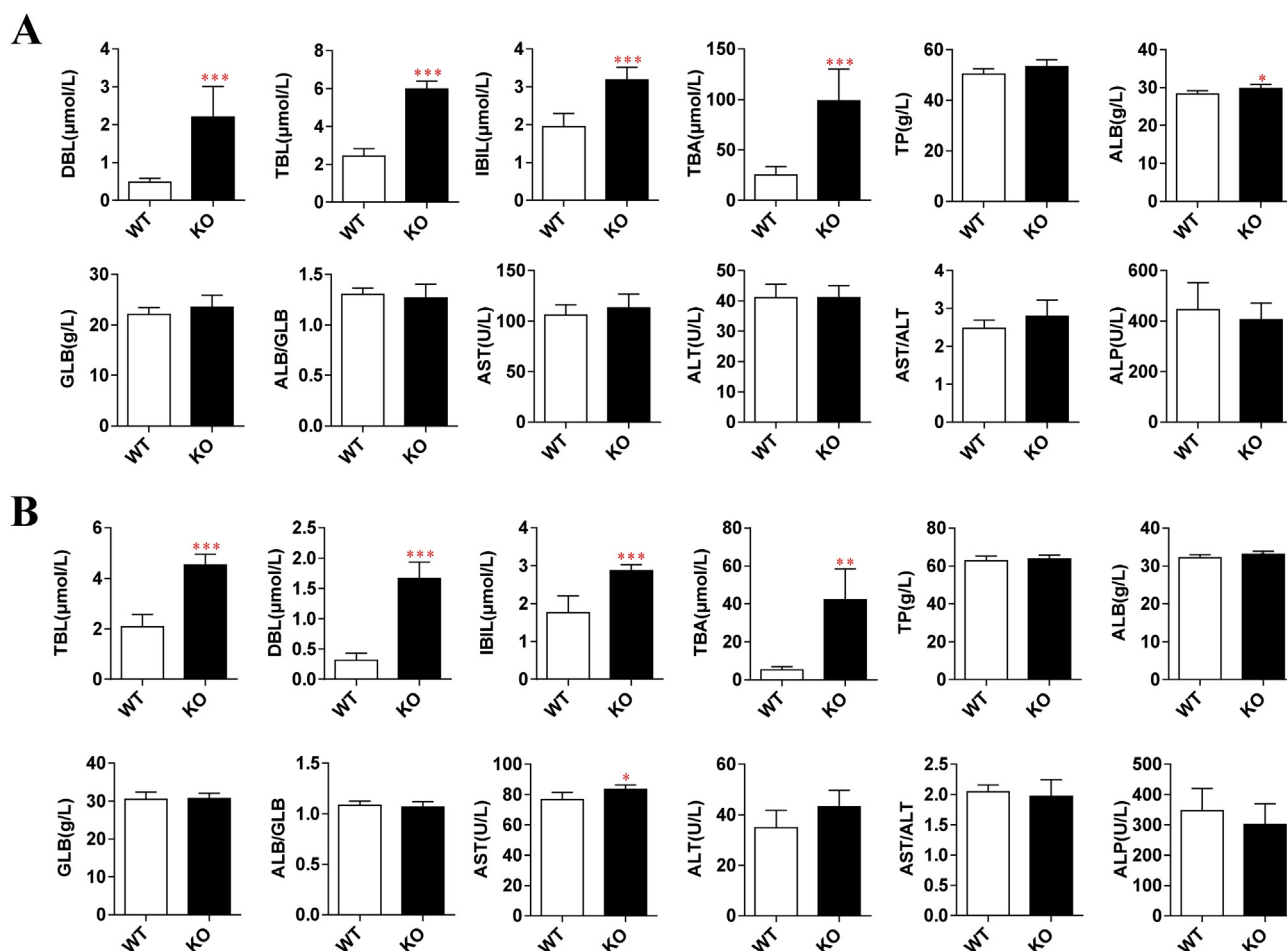
Figure 4 Indicators of liver function in WT and KO male rats. Liver function indicators in (A) 4-week-old and (B) 8-week-old WT and KO male rats ($n = 6$). Indicators include TBL, DBL, IBIL, TBA, TP, ALB, GLB, ALB/GLB, AST, ALT, AST/ALT, and ALP. Values are presented as mean $\pm$ SD ($n = 6$). $^*P < 0.05$, $^{**}P < 0.01$ and $^{***}P < 0.001$ compared with WT rats.

absorption and AUC. Despite of relatively large individual deviation, KO and WT rats still showed significant differences in the pharmacokinetic parameters. The $AUC_{0-24\ h}$ and AUC_{0-inf} of KO rats were significantly increased by both 68.8%, while the V_d/F and CL/F were significantly decreased by 39.8% and 38.5%, respectively (Table 3). In addition, T_{max}, C_{max} and MRT had trends of increase, while $t_{1/2}$ was not significantly changed. In fact, pitavastatin was uptaken into the hepatocytes by OATP1B2, and then excreted into the bile by P-gp and BCRP in WT rat livers[40]. In contrast, pitavastatin uptake in the liver of KO rats was significantly reduced, and thus the drug molecules were more likely to be retained in the bloodstream, resulting in a smaller value of V_d. At the same time, hepatic efflux transporters were hardly saturated in KO rats because the hepatic pitavastatin influx rate was significantly lower. If the hepatic clearance of pitavastatin remained unchanged, the unchanged systemic elimination rate constant k_e resulted in similar $t_{1/2}$ of the WT and KO rats, as well as the lower CL/F in KO rats decided by smaller V_d. Based on the mentioned above, the *Slco1b2* KO rat model was successfully constructed because of the loss of expression and function of *Oatp1b2*.

In the process of developing new drugs, we can compare the pharmacokinetic profiles of the tested compounds or specific substrates in WT and KO rats to determine whether the drugs are substrates, inhibitors or inducers of OATP1B2. Careful

conclusions could be further extrapolated to human OATP1B1/3, especially OATP1B1/3-mediated drug transport and drug−drug interactions. Compared with cell models, the results from the rat model can provide more information about the significance of the influx transporter on systemic exposure of the drug at an integrate level. Although *Oatp1b2* KO mice model was constructed, mRNA levels of other transporters such as *Oatp1a4*, *Oat2* and *Mrp3* were significantly changed[22]. Therefore, the *Oatp1b2* KO rats were a better model to study the function of OATP1B2 than the mice model because of no changes of other transporters. Moreover, adverse drug reactions (ADRs) caused by inter-patient differences in drug responsiveness affect 2%−6% of hospitalized patients, mainly due to genetic polymorphism[41]. Actually, there are 10 single nucleotide polymorphisms (SNPs) of *SLCO1B1* to decrease the activity of OATP1B1, among which the most common and influential are the c.512T > C and c.388A > G. The *SLCO1B3* c.334T > G and c.699G > A SNPs decrease the transport capacity[42,43]. Therefore, the *Slco1b2* KO rat model could be used for pre-clinical pharmacokinetic experiments to provide some support for personalized medication for patients with *SLCO1B1 and SLCO1B3* SNPs.

On the other hand, this *Slco1b2* KO model can be used in cancer-related research, because the OATP research has gradually associated with drug resistance and target therapy in recent years[44]. The low expression of OATP1B1 or OATP1B3 often leads
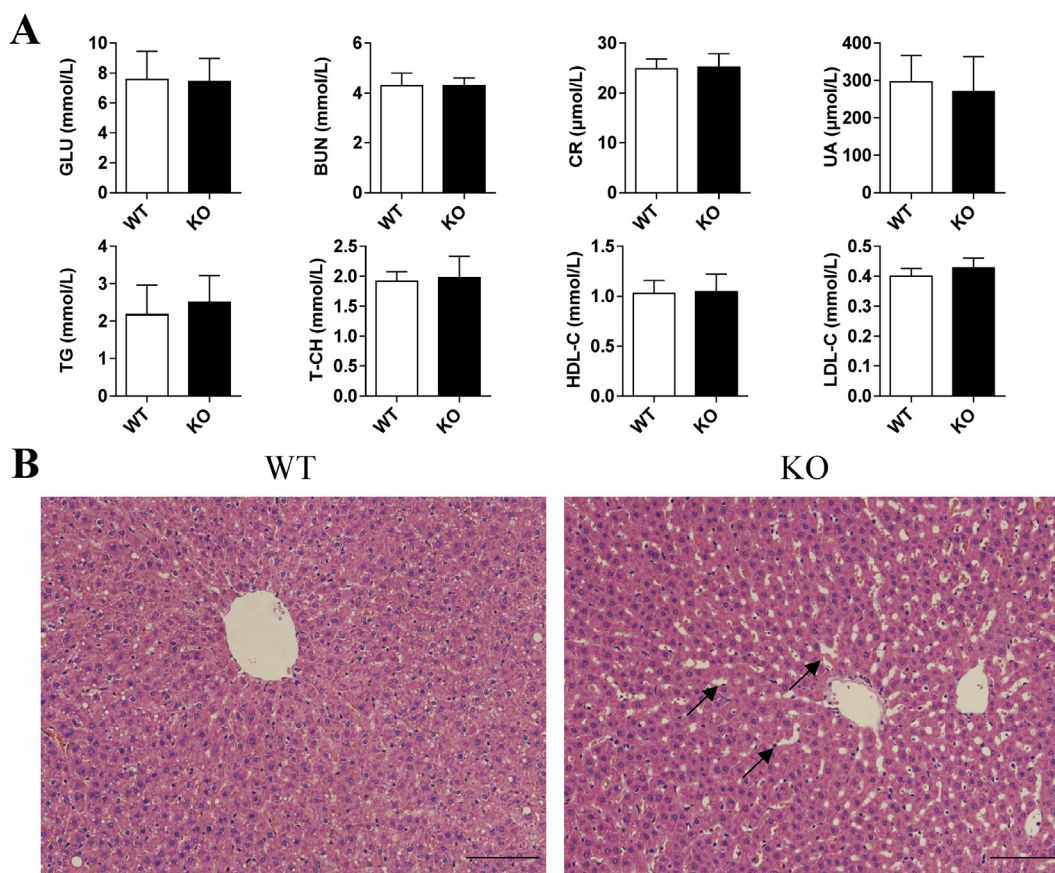
Figure 5 Physiological phenotype in WT and KO male rats. (A) Glucose, renal function and blood lipids indexes in 8-week-old WT and KO rats. Indicators include GLU, BUN, CR, UA, TG, T-CH, HDL-C, and LDL-C. Values are shown as mean ± SD ($n = 6$). (B) HE staining for liver sections in 8-week-old rats. The cytoplasm was stained mauve by eosin, and the cell nucleus was stained blue by hematoxylin. Scale bars, 100 μm in length.

to the decrease of intracellular drug concentrations, which results in drug resistance[32]. In contrast, overexpression of OATP1B1 or OATP1B3 in drug-resistant cells can reverse the resistance to a certain extent and enhance the therapeutic effects[45]. In addition, OATP1B1 and OATP1B3 are almost specifically expressed in the liver under normal conditions, but in some tumors they are not only expressed, but also expressed differently at different stages of tumors[5,46,47]. These specific mechanisms are not clear yet, but it can be used as a potential target to provide new ideas for cancer treatment[46]. Therefore, the *Slco1b2* KO rat model is a powerful experimental tool to explore the relationship between OATP1B1/3 and tumors.

The *Slco1b2* KO rats are capable of not only making contribution to drug evaluation[48], but also serving as a disease model. For example, there are many causes of hyperbilirubinemia. At present, different animal models have been established to simulate hyperbilirubinemia, such as intraperitoneal or intravenous injection of bilirubin into neonatal rats, which results in the increase of bilirubin content in rats; or the construction of a UDP glucuronosyltransferase family 1 member A1 (*Ugt1a1*) gene KO mouse model to simulate neonatal jaundice[49−51]. But there is no disease model of Rotor syndrome to date. In this study, the *Slco1b2* KO rat model presented the same pathogenesis and disease characteristics as clinical Rotor syndrome. For example, the total bilirubin (TBL) and direct bilirubin (DBL) in the serum of KO rats were significantly higher than those in WT rats (Fig. 4). These results are consistent with the symptoms caused by the absence of OATP1B1

and OATP1B3 in Rotor syndrome[14]. Therefore, the *Slco1b2* KO rat model can be used as a disease model of Rotor syndrome and hyperbilirubinemia, as well as the hyperbilirubinemia-related diseases.

Since Rotor syndrome is a kind of jaundice in children and adolescents, we detected the physiological indexes of liver function in serum of 4-week-old KO rats and WT rats. The results
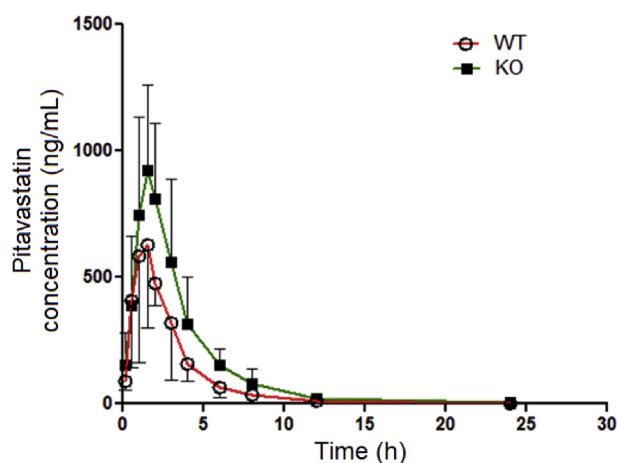

Figure 6 Pharmacokinetics of pitavastatin in WT and KO rats. The concentrations of pitavastatin were determined by LC−MS/MS. Values are presented as mean ± SD ($n = 6$).

Table 3 Pharmacokinetic parameters of pitavastatin after oral administration.

Parameter	Unit	WT	KO
$t_{1/2}$	h	2.98 ± 0.62	2.92 ± 0.43
T_{max}	h	1.58 ± 0.86	2.08 ± 0.97
C_{max}	ng/mL	757.70 ± 316.98	1001.32 ± 335.82
AUC_{0-t}	h·ng/mL	2022.50 ± 393.63	$3414.25 \pm 1041.89^{*}$
AUC_{0-inf}	h·ng/mL	2037.19 ± 368.42	$3439.51 \pm 1051.67^{*}$
V_d/F	mL/kg	10931.16 ± 3360.51	$6580.87 \pm 1897.02^{*}$
CL/F	mL/h/kg	2539.70 ± 572.91	$1562.04 \pm 430.31^{**}$
MRT_{0-t}	h	3.01 ± 0.84	3.65 ± 0.89

The dose was 5 mg/kg (*p.o.*). Results were mean $\pm$ SD ($n = 6$). $^{*}P < 0.05$, and $^{**}P < 0.01$ compared to WT rats.

showed that TBL, DBL, IBIL and TBA in KO rats were significantly higher than those in WT rats. But these phenomena still existed in 8-week-old rats. At the same time, HE staining showed that the structure of hepatocytes was blurred, the arrangement was disordered and the hepatic sinusoids were enlarged in the liver tissue sections of KO rats. These results indicated that hyperbilirubinemia has accompanied the growth of rats. Probably due to the long-term exposure of hyperbilirubinemia environment, liver cells were damaged to a certain extent. The total bile acid content in KO rats was significantly increased, because the bile acids were the substrate for *Oatp1b2*[52]. The loss of *Oatp1b2* function resulted in the accumulation of total bile acids in the blood. These results suggest the long-term monitoring of hepatic function in patients with Rotor syndrome is necessary, and the high risks of hepatocyte lesions as well as cholestasis should be noticed.

In summary, the *Slco1b2* KO rat model was successfully constructed by CRISPR/Cas9 technology, with no off-target and compensatory effects. This rat model can be used in pharmacokinetic research. At the same time, this model presents the disease characteristics of hyperbilirubinemia-Rotor syndrome, especially caused by the absence of OATP1B1/3. Thus this model can also be used as a disease model to study hyperbilirubinemia-related diseases.

Acknowledgments

Author contributions

Xin Wang was responsible for the conception and design of the study. Xinrun Ma, Xuyang Shang, Xuan Qin, and Jian Lu performed experiments. Xinrun Ma, Xuyang Shang and Xin Wang analyzed results and interpreted data. Xinrun Ma, Xuyang Shang, Xuan Qin, and Jian Lu drafted the manuscript. Mingyao Liu and Xin Wang revised the manuscript.

Conflicts of interest

The authors declare no conflicts of interest.

Appendix A. Supporting information

Supporting data to this article can be found online at https://doi.org/10.1016/j.apsb.2019.11.007.

References

1. Wolkoff AW. Organic anion uptake by hepatocytes. *Comp Physiol* 2014;**4**:1715−35.
2. Hagenbuch B, Stieger B. The *SLCO* (former *SLC21*) superfamily of transporters. *Mol Asp Med* 2013;**34**:396−412.
3. Roth M, Obaidat A, Hagenbuch B. OATPs, OATs and OCTs: the organic anion and cation transporters of the *SLCO* and *SLC22A* gene superfamilies. *Br J Pharmacol* 2012;**165**:1260−87.
4. Abe T, Unno M, Onogawa T, Tokui T, Kondo TN, Nakagomi R, et al. LST-2, a human liver-specific organic anion transporter, determines methotrexate sensitivity in gastrointestinal cancers. *Gastroenterology* 2001;**120**:1689−99.
5. Thakkar N, Lockhart AC, Lee W. Role of organic anion-transporting polypeptides (OATPs) in cancer therapy. *AAPS J* 2015;**17**:535−45.
6. Maeda K. Organic anion transporting polypeptide (OATP)1B1 and OATP1B3 as important regulators of the pharmacokinetics of substrate drugs. *Biol Pharm Bull* 2015;**38**:155−68.
7. Stieger B, Hagenbuch B. Organic anion-transporting polypeptides. *Curr Top Membr* 2014;**73**:205−32.
8. Sissung TM, Reece KM, Spencer S, Figg WD. Contribution of the OATP1B subfamily to cancer biology and treatment. *Clin Pharmacol Ther* 2012;**92**:658−60.
9. Karlgren M, Vildhede A, Norinder U, Wisniewski JR, Kimoto E, Lai Y, et al. Classification of inhibitors of hepatic organic anion transporting polypeptides (OATPs): influence of protein expression on drug−drug interactions. *J Med Chem* 2012;**55**:4740−63.
10. Shitara Y. Clinical importance of OATP1B1 and OATP1B3 in drug−drug interactions. *Drug Metab Pharmacokinet* 2011;**26**:220−7.
11. International Transporter Consortium, Giacomini KM, Huang SM, Tweedie DJ, Benet LZ, Brouwer KL, et al. Membrane transporters in drug development. *Nat Rev Drug Discov* 2010;**9**:215−36.
12. U.S. Food and Drug Administration. *Guidance for industry: in vitro metabolism and transporter mediated drug−drug interaction studies*. Available from: https://www.federalregister.gov/documents/2017/10/25/2017-23102/in-vitro-metabolism--and-transporter-mediated-drug-drug-interaction-studies-and-clinical-drug.
13. Dhumeaux D, Erlinger S. Hereditary conjugated hyperbilirubinaemia: 37 years later. *J Hepatol* 2013;**58**:388−90.
14. van de Steeg E, Stránecký V, Hartmannová H, Nosková L, Hřebíček M, Wagenaar E, et al. Complete OATP1B1 and OATP1B3 deficiency causes human Rotor syndrome by interrupting conjugated bilirubin reuptake into the liver. *J Clin Investig* 2012;**122**:519−28.
15. Green SM, Kaipainen A, Bullock K, Zhang A, Lucas JM, Matson C, et al. Role of OATP transporters in steroid uptake by prostate cancer cells *in vivo*. *Prostate Cancer Prostatic Dis* 2017;**20**:20−7.
16. Hamada A, Sissung T, Price DK, Danesi R, Chau CH, Sharifi N, et al. Effect of *SLCO1B3* haplotype on testosterone transport and clinical outcome in caucasian patients with androgen-independent prostatic cancer. *Clin Cancer Res* 2008;**14**:3312−8.
17. Yang M, Xie W, Mostaghel E, Nakabayashi M, Werner L, Sun T, et al. SLCO2B1 and SLCO1B3 may determine time to progression for patients receiving androgen deprivation therapy for prostate cancer. *J Clin Oncol* 2011;**29**:2565−73.
18. van de Steeg E, Wagenaar E, van der Kruijssen CM, Burggraaff JE, de Waart DR, Elferink RP, et al. Organic anion transporting polypeptide 1a/1b-knockout mice provide insights into hepatic handling of bilirubin, bile acids, and drugs. *J Clin Investig* 2010;**120**:2942−52.
19. Gonzalez FJ, Fang ZZ, Ma X. Transgenic mice and metabolomics for study of hepatic xenobiotic metabolism and toxicity. *Expert Opin Drug Metab Toxicol* 2015;**11**:869−81.

20. Hagenbuch B, Gui C. Xenobiotic transporters of the human organic anion transporting polypeptides (OATP) family. *Xenobiotica* 2008;**38**: 778−801.

21. Lu H, Choudhuri S, Ogura K, Csanaky IL, Lei X, Cheng X, et al. Characterization of organic anion transporting polypeptide 1b2-null mice: essential role in hepatic uptake/toxicity of phalloidin and microcystin-LR. *Toxicol Sci* 2008;**103**:35−45.

22. Zaher H, Meyer zu, Schwabedissen HE, Tirona RG, Cox ML, Obert LA, Agrawal N, et al. Targeted disruption of murine organic anion-transporting polypeptide 1b2 (*Oatp1b2/Slco1b2*) significantly alters disposition of prototypical drug substrates pravastatin and rifampin. *Mol Pharmacol* 2008;**74**:320−9.

23. Shapiro SM. Bilirubin toxicity in the developing nervous system. *Pediatr Neurol* 2003;**29**:410−21.

24. Mikkaichi T, Nakai D, Yoshigae Y, Imaoka T, Okudaira N, Izumi T. Liver-selective distribution in rats supports the importance of active uptake into the liver *via* organic anion transporting polypeptides (OATPs) in humans. *Drug Metab Pharmacokinet* 2015;**30**:334−40.

25. Cong L, Ran FA, Cox D, Lin S, Barretto R, Habib N, et al. Multiplex genome engineering using CRISPR/Cas systems. *Science* 2013;**339**:819−23.

26. Mali P, Yang L, Esvelt KM, Aach J, Guell M, DiCarlo JE, et al. RNA-guided human genome engineering *via* Cas9. *Science* 2013;**339**: 823−6.

27. Jiang F, Doudna JA. CRISPR-Cas9 structures and mechanisms. *Annu Rev Biophys* 2017;**46**:505−29.

28. Ceasar SA, Rajan V, Prykhozhij SV, Berman JN, Ignacimuthu S. Insert, remove or replace: a highly advanced genome editing system using CRISPR/Cas9. *Biochim Biophys Acta* 2016;**1863**:2333−44.

29. Liu X, Wu S, Xu J, Sui C, Wei J. Application of CRISPR/Cas9 in plant biology. *Acta Pharm Sin B* 2017;**7**:292−302.

30. Luo Z, Zhang Y, Gu J, Feng P, Wang Y. Pharmacokinetic properties of single- and multiple-dose pitavastatin calcium tablets in healthy Chinese volunteers. *Curr Ther Res Clin Exp* 2015;**77**:52−7.

31. Niemi M, Pasanen MK, Neuvonen PJ. Organic anion transporting polypeptide 1B1: a genetically polymorphic transporter of major importance for hepatic drug uptake. *Pharmacol Rev* 2011;**63**:157−81.

32. de Morrée ES, Böttcher R, van Soest RJ, Aghai A, de Ridder CM, Gibson AA, et al. Loss of SLCO1B3 drives taxane resistance in prostate cancer. *Br J Canc* 2016;**115**:674−81.

33. Ulvestad M, Darnell M, Molden E, Ellis E, Åsberg A, Andersson TB. Evaluation of organic anion-transporting polypeptide 1B1 and CYP3A4 activities in primary human hepatocytes and HepaRG cells cultured in a dynamic three-dimensional bioreactor system. *J Pharmacol Exp Ther* 2012;**343**:145−56.

34. Qin X, Wang X. Role of vitamin D receptor in the regulation of *CYP3A* gene expression. *Acta Pharm Sin B* 2019;**9**:1087−98.

35. Zhang J, Wang C, Liu Q, Meng Q, Cang J, Sun H, et al. Pharmacokinetic interaction between JBP485 and cephalexin in rats. *Drug Metab Dispos* 2010;**38**:930−8.

36. Liang C, Zhao J, Lu J, Zhang Y, Ma X, Shang X, et al. Development and characterization of *MDR1* (*Mdr1a/b*) CRISPR/Cas9 knockout rat model. *Drug Metab Dispos* 2019;**47**:71−9.

37. Qin X, Lu J, Wang P, Xu P, Liu M, Wang X. Cytochrome P450 3A selectively affects the pharmacokinetic interaction between erlotinib and docetaxel in rats. *Biochem Pharmacol* 2017;**143**:129−39.

38. Wang X, Tang Y, Lu J, Shao Y, Qin X, Li Y, et al. Characterization of novel cytochrome P450 2E1 knockout rat model generated by CRISPR/Cas9. *Biochem Pharmacol* 2016;**105**:80−90.

39. Wang HX, Li M, Lee CM, Chakraborty S, Kim HW, Bao G, et al. CRISPR/Cas9-based genome editing for disease modeling and therapy: challenges and opportunities for nonviral delivery. *Chem Rev* 2017;**117**:9874−906.

40. Prueksaritanont T, Chu X, Evers R, Klopfer SO, Caro L, Kothare PA, et al. Pitavastatin is a more sensitive and selective organic anion-transporting polypeptide 1B clinical probe than rosuvastatin. *Br J Clin Pharmacol* 2014;**78**:587−98.

41. Scott SA. Personalizing medicine with clinical pharmacogenetics. *Genet Med* 2011;**13**:987−95.

42. Gong IY, Kim RB. Impact of genetic variation in OATP transporters to drug disposition and response. *Drug Metab Pharmacokinet* 2013;**28**: 4−18.

43. Niemi M, Backman JT, Kajosaari LI, Leathart JB, Neuvonen M, Daly AK, et al. Polymorphic organic anion transporting polypeptide 1B1 is a major determinant of repaglinide pharmacokinetics. *Clin Pharmacol Ther* 2005;**77**:468−78.

44. König SK, Herzog M, Theile D, Zembruski N, Haefeli WE, Weiss J. Impact of drug transporters on cellular resistance towards saquinavir and darunavir. *J Antimicrob Chemother* 2010;**65**:2319−28.

45. Herraez E, Sanchez-Vicente L, Macias RIR, Briz O, Marin JJG. Usefulness of the MRP2 promoter to overcome the chemoresistance of gastrointestinal and liver tumors by enhancing the expression of the drug transporter OATP1B1. *Oncotarget* 2017;**8**:34617−29.

46. Teft WA, Welch S, Lenehan J, Parfitt J, Choi YH, Winquist E, et al. OATP1B1 and tumour OATP1B3 modulate exposure, toxicity, and survival after irinotecan-based chemotherapy. *Br J Canc* 2015;**112**: 857−65.

47. Wright JL, Kwon EM, Ostrander EA, Montgomery RB, Lin DW, Vessella R, et al. Expression of *SLCO* transport genes in castration-resistant prostate cancer and impact of genetic variation in *SLCO1B3* and *SLCO2B1* on prostate cancer outcomes. *Cancer Epidemiol Biomark Prev* 2011;**20**:619−27.

48. Ma X, Qin X, Shang X, Liu M, Wang X. Organic anion transport polypeptide 1b2 selectively affects the pharmacokinetic interaction between paclitaxel and sorafenib in rats. *Biochem Pharmacol* 2019; **169**:113612.

49. Rice AC, Shapiro SM. A new animal model of hemolytic hyperbilirubinemia-induced bilirubin encephalopathy (kernicterus). *Pediatr Res* 2008;**64**:265−9.

50. Hansen T, Tommarello S, Allen J. Subcellular localization of bilirubin in rat brain after *in vivo* i.v. administration of [^{3}H]bilirubin. *Pediatr Res* 2001;**49**:203−7.

51. Porro F, Bockor L, De Caneva A, Bortolussi G, Muro AF. Generation of *Ugt1*-deficient murine liver cell lines using TALEN technology. *PLoS One* 2014;**9**:e104816.

52. Slijepcevic D, Roscam Abbing RLP, Katafuchi T, Blank A, Donkers JM, van Hoppe S, et al. Hepatic uptake of conjugated bile acids is mediated by both sodium taurocholate cotransporting polypeptide and organic anion transporting polypeptides and modulated by intestinal sensing of plasma bile acid levels in mice. *Hepatology* 2017; **66**:1631−43.